Research Square

Preprints are preliminary reports that have not undergone peer review.
They should not be considered conclusive, used to inform clinical practice,
or referenced by the media as validated information.

Symmetry-Preserving Coupling of Charge Resonance and Excited-State Quinoidalization Enables Luminescence in Ortho-Disubstituted Diradicals

Juan Casado Cordon

casado@uma.es

University of Málaga https://orcid.org/0000-0003-0373-1303

Zhaoze Ding

Jilin University

Zihao Zhu

Jilin University

Xing Wang

Jilin University

Shengjie Wang

Jilin University

Yan sun

Universite Paris-Saclay https://orcid.org/0000-0003-4429-6029

Xin Ai

Hainan University

Alim Abdurahman

Jilin University https://orcid.org/0000-0003-2419-3516

Qiming Peng

Nanjing Tech University https://orcid.org/0000-0002-7558-3234

Fabrizia Negri

Univ. Bologna https://orcid.org/0000-0002-0359-0128

Article

Keywords:

Posted Date: November 23rd, 2026

DOI: https://doi.org/10.21203/rs.3.rs-11582608/v1

License: This work is licensed under a Creative Commons Attribution 4.0 International License.
Read Full License

Additional Declarations: There is **NO** Competing Interest.

Symmetry-Preserving Coupling of Charge Resonance and Excited-State Quinoidalization Enables Luminescence in Ortho-Disubstituted Diradicals

Zhaoze Ding[1,2,†] Zihao Zhu[1,†], Xing Wang[1,3], Shengjie Wang[1], Yan Sun[4], Xin Ai[2], Alim Abdurahman[1*] Qiming Peng[3*], Fabrizia Negri[5*] Juan Casado[6*]

Abstract

Quinoidal HOMO→LUMO singly excited (SE) states are intrinsically emissive in many closed-shell π-conjugated molecules, yet they are generally inaccessible in open-shell diradicals because electron correlation reorders the excited-state manifold, rendering the SE state higher than the optically inactive HOMO, HOMO→LUMO, LUMO doubly excited (DE) charge resonant (CR) state. Here we show that, in the ortho-linked TTM-based Kekulé diradical o-TPT, coupling between the radical-centered CR states and the bridge reverses the SE/DE ordering, placing the bright SE state lowest and enabling singlet luminescence. Structural, magnetic, and computational analyses reveal that o-TPT adopts a highly twisted aromatic open-shell ground-state configuration with pronounced diradical character and an almost degenerate triplet ground state. In PMMA films, o-TPT exhibits a dual-emission behavior composed of a localized TTM-like emission at 618 nm and a low-energy emission at 780 nm. Time-resolved spectroscopy, transient absorption measurements and excited-state calculations consistently demonstrate that the low-energy emission originates from the SE/CR singlet excited state, enabled by the combined effects of ortho connectivity and bridge-induced quinoidal rigidification. The resulting rigidification preserves the symmetry of the relaxed excited state, maintaining its bright SE character. Comparative studies of two structurally related diradicals further establish that the enhanced luminescence requires a subtle interplay between the nature of the bridge and the radical centers to avoid the formation of weakly emitting singlet charge transfer states. Variable-temperature and magnetoluminescence measurements reveal that the distinctive lowest singlet SE/CR quinoidal excited state additionally participates in spin-dependent relaxation processes. These findings establish ortho-disubstitution as an effective molecular design strategy for enhancing the luminescent properties of otherwise weak singlet emission by coupling electrostatic, electronic and structural features in Kekulé diradicals and demonstrate that dual emission provides a direct spectroscopic window into excited-state electronic-structure evolution in open-shell molecules.

Introduction

Photoexcitation can fundamentally reorganize molecular electronic structures, creating excited states with properties that differ dramatically from those of their ground-state counterparts.[1-3] Such transformations underpin many important photophysical phenomena, including charge transfer[4, 5], excited-state proton transfer[6], symmetry breaking,[7, 8] and conformational relaxation[9]. In aromatic closed-shell π-conjugated systems,[10, 11] photoexcitation typically drives the ground electronic state (S_0) electronic structure away from an aromatic configuration toward an emissive HOMO→LUMO quinoidal state, i.e., the S_1 excited state. This situation drastically changes in aromatic open-shell diradicals owing to the energetic reordering by electron correlation or mixing of the ionic and covalent electronic forms, always resulting in a lowest energy singlet excited state (S_1) characterized by the doubly excited (DE) HOMO, HOMO→LUMO, LUMO configuration, which makes it of the same symmetry as the ground state (S_0) and photonically inactive in centrosymmetric systems. [12, 13] As a result, the one-photon active HOMO→LUMO singly excited (SE) state becomes higher in energy (S_2) and strongly deactivated by internal conversion ($S_2 \rightsquigarrow S_1$). [14-18] This has made most known diradicals non-emissive and only recently some (with moderate diradical character) have been reshaped into emissive molecules due to the mixing between the bright SE state and the dark DE state, both characterized by a charge-resonance (CR) character, yielding a symmetry-broken optically active charge-transfer (CT) state. [19, 20] Though this strategy is a valid proof-of-concept, alternative routes to get emissive diradicals based on chemical-based design are mandatory. One major question is whether the DE/SE order can be reversed by chemical design. This is pertinent as most of the work in luminescent diradicals has been done in para-disubstituted structures. [19, 21-23].

Along these lines, we study ortho-disubstituted diradicals with which two structural aspects are tuned: i) the inter-radical coupling involved in the charge resonance (electrostatic effect) is enlarged by increasing their proximity; and, simultaneously, ii) the quinoidal form (covalent effect) is further promoted (regarding para-substitution) due to the more subtle aromatic-quinoidal balance in ortho-substitution.

Over the past decade, extensive efforts have focused on manipulating the aromatic-quinoidal balance to control diradical character,[24-26] singlet–triplet energy gaps,[27, 28] spin polarization,[29-31] and luminescence.[32, 33] Recently, concerning the singlet manifold in para-disubstituted diradicals, Mesto et al.[34] have theoretically

[1] State Key Laboratory of Integrated Optoelectronics, College of Electronic Science and Engineering, College of Integrated Circuits, Jilin University, Changchun, China. [2] School of Materials Science and Engineering, Hainan University, Haikou, Hainan, China. [3] Key Laboratory of Flexible Electronics (KLOFE), Institute of Advanced Materials (IAM) & School of Flexible Electronics (Future Technologies), Nanjing Tech University (NanjingTech), Nanjing 211816, P.R. China. [4] Laboratoire de Physique des Solides (LPS), Université Paris-Sud, Centre National de la Recherche Scientifique (CNRS), UMR 8502, F-91405 Orsay, France.4. [5] Dipartimento di Chimica "Giacomo Ciamician", Università di Bologna, Via P. Gobetti 85, 40129 Bologna (Italy); Center for Chemical Catalysis-C3, Università di Bologna, Bologna 40129, Italy and INSTM UdR Bologna, 40129, Bologna, Italy. [6] Department of Physical Chemistry, University of Malaga, Campus de Teatinos, Malaga, Spain.
*E-mail: alim@jlu.edu.cn (Alim Abdurahman); iamqmpeng@njtech.edu.cn (Qiming Peng); fabrizia.negri@unibo.it (Fabrizia Negri); casado@uma.es (Juan Casado)

shown that Chichibabin and Müller diradicals display two novel low-lying excited states, absent in TTM radicals, arising from CR between the radical units, the lowest of which is the DE state. Another recent computational study[35] has also supported the CT nature of the singlet emitting state in triarylmethyl diradicals, emphasizing the role of the bridge on the CT-state energy. Consistent with this understanding, Dong et al. [33] demonstrated that thermally accessible singlet and triplet manifolds can produce distinct $S_1 \rightarrow S_0$ and $T_1 \rightarrow T_0$ fluorescence channels in TTM diradicaloids. Kusamoto et al. [36, 37] have also reported singlet emission with zwitterionic charge-separated character in spatially confined diradicals. Overall, the present understanding of TTM-derived diradicals is that the lowest singlet emitting state has a CR/CT (or zwitterionic) character and is generally weakly emitting, or even non-emissive.

Despite these advances, a general molecular strategy for turning the intrinsically dark lowest singlet excited state into an efficiently accessible emissive state with tunable energy remains elusive. An open question is whether the energy, electronic mixing, and radiative accessibility of the lowest singlet excited state can be controlled dynamically through excited-state structural reorganization. Whether molecular topology can couple the distinctive excited state electronic structure of diradicals to a defined structural relaxation coordinate, thereby stabilizing/tuning the energy and activating the lowest singlet state emission, while preserving an independent triplet emission channel, remains unexplored. The ortho connectivity offers a particularly attractive platform to test these ideas because, as mentioned before, it simultaneously modifies radical–radical proximity, through-bond coupling, conformational flexibility, and the accessible aromatic-to-quinoidal relaxation coordinate.

Hence, herein, we exploit an ortho-linked TTM-based Kekulé diradical in order to demonstrate that provides an ideal platform for directly capturing such coupling between the electronic identity of the singlet emitting state and its structural reorganization (excited-state quinoidization) for directly tuning dual emission. Single-crystal analysis reveals a twisted aromatic open-shell geometry while EPR and SQUID measurements establish a triplet ground state with an almost degenerate singlet state. Remarkably, o-TPT exhibits dual emission in PMMA films, arising from two distinct excited-state relaxation pathways. Combined transient spectroscopy, control-molecule studies, and theoretical calculations reveal that photoexcitation triggers a structural relaxation toward a quinoidal excited-state structure, driven by the ortho connection, thereby opening an improved low-energy emissive channel in the singlet manifold driven by DE / SE state inversion. These results provide direct insight into the excited-state evolution and tuning of Kekulé diradicals by molecular chemical design and establish the coupling between charge resonance and quinoidalization-induced excited-state rigidification as fundamental excited-state design elements that enable inversion of the SE/DE state ordering and subsequent luminescence in ortho-substituted open-shell molecules.

Results

Aromatic Open-Shell Ground State

To investigate the origin of the proposed coupling between structural (quinoidization) and electronic (DE/CR character) excited-state properties, we first designed and synthesized the target molecule. The synthetic routes and characterization data are provided in the (Supporting Information Section 1). Single crystals suitable for X-ray diffraction were obtained by slow evaporation from a dichloromethane/methanol mixed solvent (Supporting Information Section 2). As shown in (Fig. 1a), o-TPT adopts a markedly twisted molecular geometry, in sharp contrast to the nearly planar quinoidal structures commonly observed in classical para-substituted Kekulé diradicals[19, 21-23] such as Chichibabin and Thiele-type hydrocarbons. The central phenylene ring forms dihedral angles of 41.5° and 50.8° with the adjacent aryl units of TTM (Fig. 1a), indicating substantial steric driven distortion.

This unusual geometry is accompanied by pronounced aromatic character in the benzene rings in the ground electronic state. Harmonic Oscillator Model of Aromaticity (HOMA) analysis reveals high aromaticity values for rings A-C (0.95, 0.94, and 0.96, respectively in Supplementary Fig. 5).[24, 27] Consistently, DFT calculations yield a diradical character index of 0.919 (Supplementary Table. 6), substantially larger than those reported for many Chichibabin- and Thiele-type Kekulé diradicals. [21, 22, 32, 38-43] Taken together, these structural and theoretical analyses establish o-TPT as a highly twisted aromatic species in the ground state.

While these structural analyses establish the aromatic character of o-TPT, its spin state and open-shell character require further experimental verification. Electrochemical measurements reveal that, in stark contrast to the single redox couple observed for o-HTPT, o-TPT exhibits two distinct redox peaks in its cyclic voltammogram, either in oxidation and in reduction (Supplementary Fig. 6), corresponding to the sequential one-electron transfer processes on the two unpaired electrons within the diradical. The splitting of the two anodic and cathodic waves indicates the simultaneous action of inter-radical charge delocalization and direct charge repulsion in the divalent species (i.e., dication and dianion). The first insight agrees with the singlet open-shell diradical character due to effective overlap through ortho-conjugation. Continuous-wave electron paramagnetic resonance (CW-EPR) measurements show characteristic signatures of an open-shell species in both PMMA films and solution (Figs. 1b, d). More importantly, a distinct half-field transition ($\Delta ms = \pm 2$) is observed in PMMA films (see inset of Fig. 1b), providing strong spectroscopic evidence for the existence of a triplet diradical species. In contrast, the corresponding monoradical o-HTPT displays only a single resonance signal and shows no detectable half-field transition under identical conditions (Fig. 1d), consistent with its monoradical structure revealed by single-crystal analysis (Fig. 1c). The EPR spectrum of a 0.1 wt% doped sample was simulated using the EasySpin software to extract the dipolar coupling constant $|D/hc|$ and the asymmetry parameter $|E/hc|$, which describes the distribution of spin density (Supplementary Fig. 7). The fitting yields zero-field splitting parameters of $|D| = 131.6$ MHz and $|E| = 13.44$ MHz. Combined with the point-dipole approximation[41], the spin-spin distance is estimated to be 8.38 Å from the $|D|$ value, which is close to the C_1-C_{16} atomic distance of 8.11 Å determined by X-ray structural analysis (Supplementary Fig. 5).

VT-EPR measurements (Fig. 1e and Supplementary Fig. 8) have been further carried out. The intensity of the half-field signal

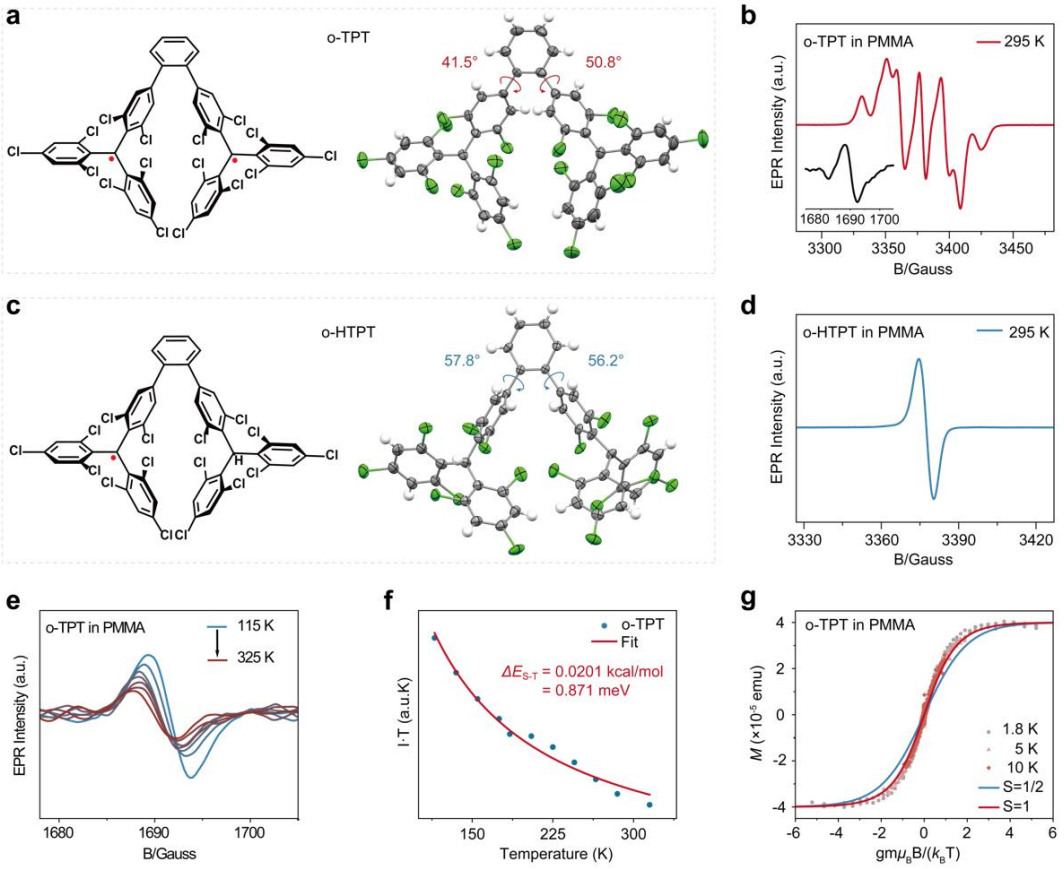


Fig. 1 | Structures and magnetic properties of the mono- and diradical. a, Molecular and crystal structures of o-TPT. **b**, EPR spectra of 0.1 wt% o-TPT (the inset shows the Δms = ± 2 resonance) doped in PMMA at room temperature. **c**, Molecular and crystal structures of o-HTPT. **d**, EPR spectra of 0.1 wt% o-HTPT doped in PMMA at room temperature. **e**, Half-field variable-temperature (VT) EPR spectra of 0.1 wt% o-TPT doped in PMMA from 115 K to 325 K; **f**, The IT-T relationship curve fitted by the Bleaney-Bowers equation. **g**, Magnetic field dependence of magnetization (M) for the doped PMMA sample measured at 1.8 K (circles), 5 K (squares), and 10 K (triangles). The solid lines represent the simulated curves for S = 1/2 (blue) and S = 1 (red).

decreases progressively with increasing temperature, consistent with thermal population redistribution between triplet and singlet spin manifolds. Fitting the temperature-dependent signal intensity using the Bleaney-Bowers model affords a singlet-triplet energy gap ($\Delta E_{S\text{-}T}$) of 0.0201 kcal mol^{-1} (0.871 meV), indicating a triplet ground state separated from the singlet state by only a very small energy difference (Fig. 1f). SQUID magnetometry (Fig. 1g) supports the behavior expected for a weakly coupled triplet diradical and is in good agreement with the $\Delta E_{S\text{-}T}$ value obtained from EPR analysis. The consistency between the crystallographic, EPR, magnetic, and theoretical analyses provides a coherent picture of the ground-state electronic structure of o-TPT as an admixture of singlet and triplet states in thermal equilibrium.

Photophysical Properties of o-TPT: Dual Emission Behavior

Despite the pronounced diradical character of o-TPT, both o-TPT and o-HTPT exhibit similar absorption profiles. In methylcyclohexane solution (Fig 2a), o-TPT exhibits an emission maximum at 616 nm, while the monoradical o-HTPT displays a slightly blue-shifted emission at 613 nm. TD-DFT calculations of the absorption spectra for both o-TPT and o-HTPT are in excellent agreement with the experimental data (Supplementary Fig. 21). The calculations further reveal that the main features of the $S_1 \rightarrow S_n$ and $T_1 \rightarrow T_n$ absorption spectra are highly comparable. The computed excitation energies and oscillator strengths (Supplementary Table. 7), together with the natural transition orbital (NTO) analysis of the most relevant excitations, enable a direct comparison of (i) the singlet and triplet excited-state manifolds of o-TPT and (ii) the excited states of the diradical o-TPT with those of the monoradical o-HTPT, as shown in Fig 3a.

The NTO analysis establishes the electronic character of the excited states and provides a direct correspondence between the excited-state manifolds of the diradical and monoradical species which are essential to discuss the photoinduced processes. Accordingly, the intense absorption band observed experimentally in the compounds at approximately 375 nm can be assigned to $S_0 \rightarrow S_{15}$ excitation in the singlet manifold of o-TPT, to the $T_0 \rightarrow T_{13}$ for the triplet species and to the $D_0 \rightarrow D_7$ transition in o-HTPT, all of which are predicted to possess significant oscillator strengths (together with additional states omitted from Fig 3a for clarity). These excitations all exhibit the same local excitation (LE) character. The weak absorption band centered around 550 nm in o-TPT and in o-HTPT can be attributed to lower-energy LE states, namely $S_0 \rightarrow S_3$, $T_0 \rightarrow T_1$ and $D_0 \rightarrow D_1$, which share the same orbital character and

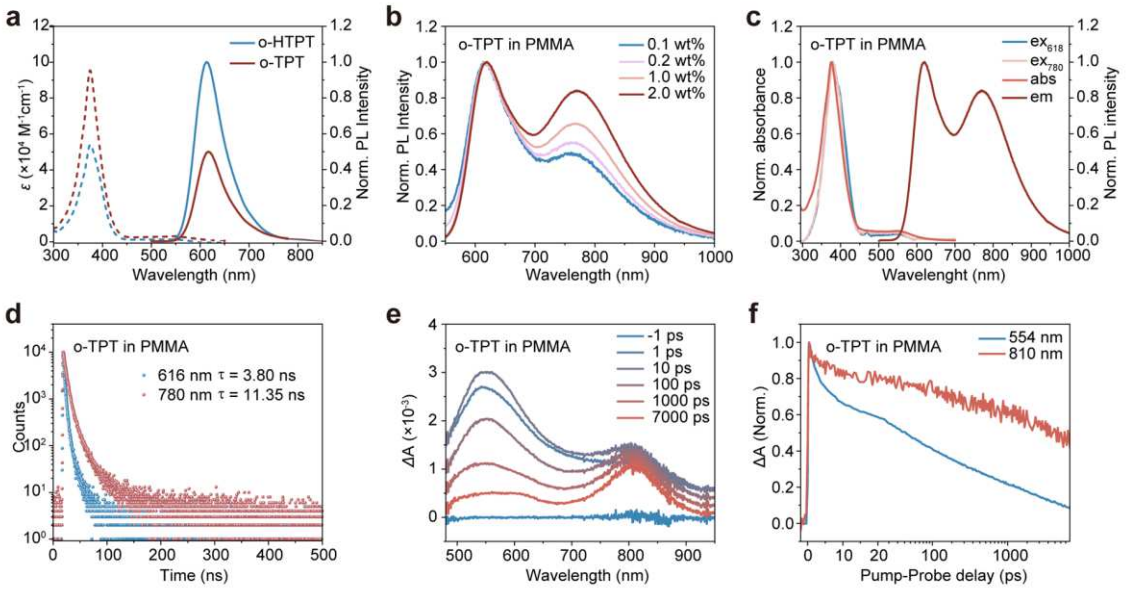


Fig. 2 | Photophysics of the luminescent diradicals. a, UV-vis absorption and Photoluminescence (PL) spectra (excitation at 375 nm) of o-TPT and o-HTPT in methylcyclohexane (10^{-5} M) at room temperature. **b**, PL spectra of o-TPT in PMMA films at varied concentrations (0.1-2 wt%) at room temperature. **c**, Excitation, absorption and emission spectra of 2 wt% o-TPT in PMMA. **d**, Time-resolved PL decay spectra (excitation at 375 nm) of 2 wt% o-TPT in PMMA, monitored at 616 and 780 nm at room temperature. **e**, Transient absorption spectra of 2 wt% o-TPT in PMMA after excitation at 375 nm. **f**, Kinetic fitting for 2 wt% o-TPT in PMMA at 554 nm and 810 nm.

display oscillator strengths consistent with the experimental observations. In addition, the singlet manifold of o-TPT contains two distinct excited states with pronounced charge-resonance (CR) character belonging to the SE (S_2) and DE (S_1) states which have not analogue in its triplet manifold or in o-HTPT. The theoretical analysis in Fig 3a assigns the 618 nm emission of the diradical to the $T_1 \rightarrow T_0$ fluorescence. Its emission energy closely matches that of the doublet emission, consistent with the nearly identical electronic character of the two transitions.

A striking different behavior emerges in PMMA films. Whereas o-HTPT displays a single TTM-based emission band across the entire concentration range investigated (Supplementary Fig. 13), o-TPT exhibits a distinctive dual-emission feature composed of a high-energy band centered at approximately 618 nm and a second low-energy band around 780 nm (Fig 2b). Both emission bands provide excitation spectra that are fully coincident with the absorption features of o-TPT (Fig 2c). Notably, the low-energy emission is already observable at a concentration as low as 0.1 wt%, where intermolecular radical-radical interactions are expected to be negligible. In stark contrast, o-TPT in methylcyclohexane solution exhibits no detectable 780 nm low-energy feature across the concentration range from 10^{-6} to 10^{-3} M (Supplementary Fig. 14), in accordance with the absence of a conventional excimer origin, which typically requires substantially higher concentrations. [44, 45]

A behavior comparable to PMMA films is found for the low-temperature measurements in methylcyclohexane solution of o-TPT. Upon cooling to 80 K, o-TPT develops a distinct additional low-energy emission band around 760 nm that is absent at room temperature, whereas the monoradical o-HTPT continues to display only a single emission band under identical conditions (Supplementary Fig. 16). In line with these studies and supported by the low-lying singlet excited-state manifold shown in Fig 3a, we assign the higher-energy emission to the $T_1 \rightarrow T_0$ transition and the red-shifted band at 780 nm to the $S_1 \rightarrow S_0$ emission from the lowest energy singlet excited state of the two, assigned with charge-resonance (CR) character (S_1). Notably, however, our results differ from previous reports in that the two emission bands exhibit comparable intensities, whereas the lower-energy emission has generally been observed to be significantly weaker in other triarylmethyl diradicals.

Fluorescence lifetime analysis clearly shows different lifetimes for the two proposed triplet and singlet emission bands (Supplementary Fig. 17), supporting their assignment to a distinct emissive excited state rather than to vibronic replica. In particular, time-resolved photoluminescence measurements in a 2 wt% o-TPT/PMMA film provide a lifetime of 3.80 ns for the 618 nm band, whereas the 780 nm emission displays a substantially longer lifetime of 11.35 ns (Fig. 2d). This pronounced deactivation kinetic difference persists across the investigated concentration range (Supplementary Table. 4). According to these lifetimes, transient absorption spectroscopy discloses that following photoexcitation at 375 nm involving the singlet and triplet manifolds of o-TPT, an initial photoinduced absorption band peaking at 554 nm is detected that rapidly decays giving way to a distinct near-infrared absorption feature (the lowest singlet excited state) which gradually develops with time with maximum at 810 nm (Figs. 2e, f). These two different excited absorption lifetimes are in coherence with the emission spectra disclosing also two different fluorescence lifetimes. Owing to the small singlet–triplet energy gap, singlet and triplet ground-state species coexist in thermal equilibrium, allowing photoexcitation of both spin manifolds and giving rise to two independent emissive pathways (Fig. 3b). Within the singlet manifold, excitation in the 500–700 nm region populates the S_3 state, which is expected to undergoes rapid internal conversion through S_2 to the lowest excited

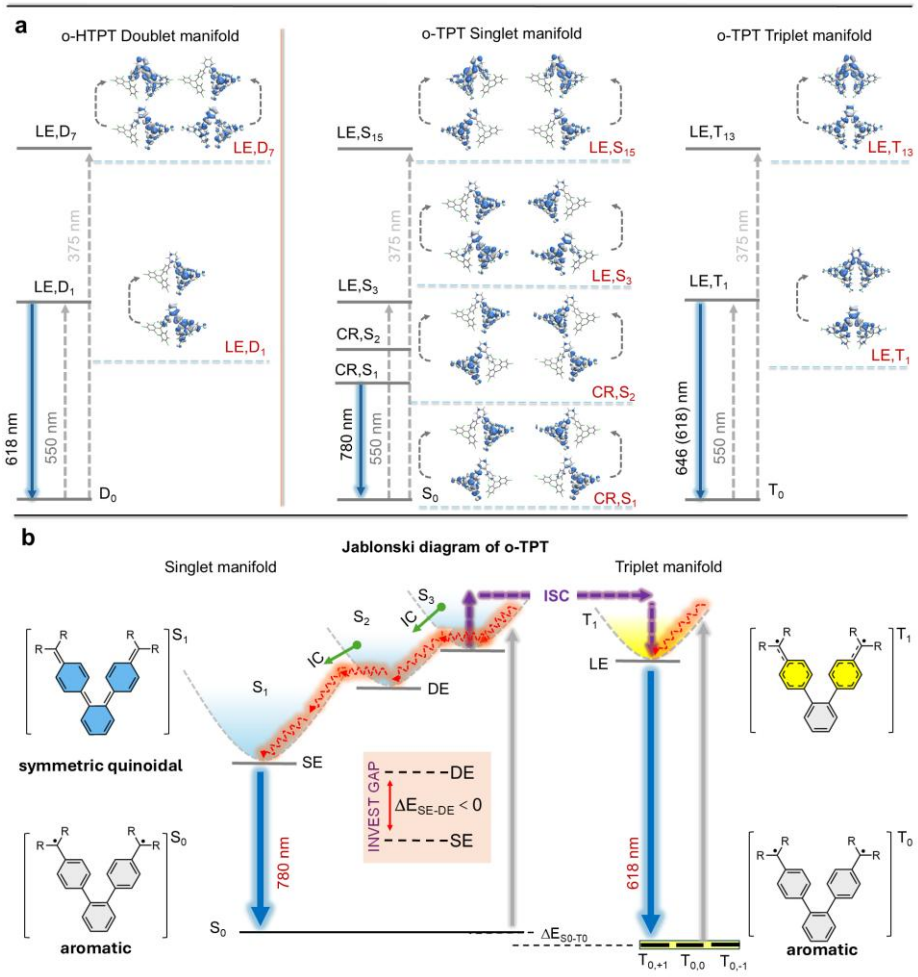


Fig. 3 | Excited-state evolution pathways of o-HTPT and o-TPT and the Jablonski diagram of o-TPT a, Comparison between the excited states in the singlet and triplet manifold of o-TPT and the doublet states of o-HTPT. The excitation energy increases from the top to the bottom. For each state, the excitations between NTO orbitals are shown. These transitions identify the character (LE or CR) of each excited state. From TD-UB3LYP/def2SVP calculations at the singlet and triplet ground state geometry of o-TPT and doublet ground state geometry of o-HTPT. **b**, Proposed Jablonski diagram illustrating the excited-state evolution pathway of o-TPT.

singlet state, S_1, from which emission occurs. In parallel, excitation of the triplet ground-state species populates T_1, which relaxes from the Franck-Condon region to its equilibrium excited-state geometry before decaying radiatively to T_0. However, the relative energies of the singlet and triplet excited states shown in Fig. 3 indicate that an additional deactivation pathway involving ISC from S_1 cannot be excluded. In particular, S_2 and S_1 are predicted to lie below T_1, whereas S_3 is nearly degenerate with T_1 providing a favorable energetic landscape for ISC.

The evolution of the lowest excited state geometries toward their equilibrium structures can be understood by considering the interaction between the radical-centered frontier orbitals (SOMOs and SUMOs) and the HOMO and LUMO of the bridge (Supplementary Fig. 22). Mixing between these orbitals modulates the excited-state character as the structure relaxes from the Franck-Condon region. At the TD-UDFT optimized geometry of the lowest triplet, the calculated $T_1 \rightarrow T_0$ emission wavelength is 643 nm (Supplementary Table. 8), in good agreement with the experimental emission maximum at 618 nm. The NTO analysis (Fig. 4f) shows that the relaxed T_1 state retains a predominantly local-excitation character on the TTM units but acquires a greater contribution from the bridge, consistent with the pronounced quinoidal distortion of the optimized structure. This increased bridge participation reflects mixing between the radical and bridge-centered frontier orbitals, facilitated by their compatible nodal patterns. The optimized T_1 state undergoes pronounced quinoidal structural relaxation, including substantial planarization of the molecular framework, enhanced bond-length alternation, and a significant decrease in HOMA values (Supplementary Fig. 26d).

For the singlet manifold, TD-UDFT calculations identify the two lowest CR states and place DE below SE, as commonly found in diradicals. However, given the sensitivity of these states to electron correlation, we re-evaluated their energies with CASSCF/NEVPT2 calculations at the ground-state geometry. To assess the effect of ortho versus para connectivity we compared o-TPT with the Müller diradical. These calculations reveal that ortho connectivity reverses the SE-DE ordering (Supplementary Table 9), placing the bright SE state below DE in o-TPT, a rarely documented inversion in diradicals. TD-UDFT does not capture this ordering, highlighting the importance of the correlated treatment in

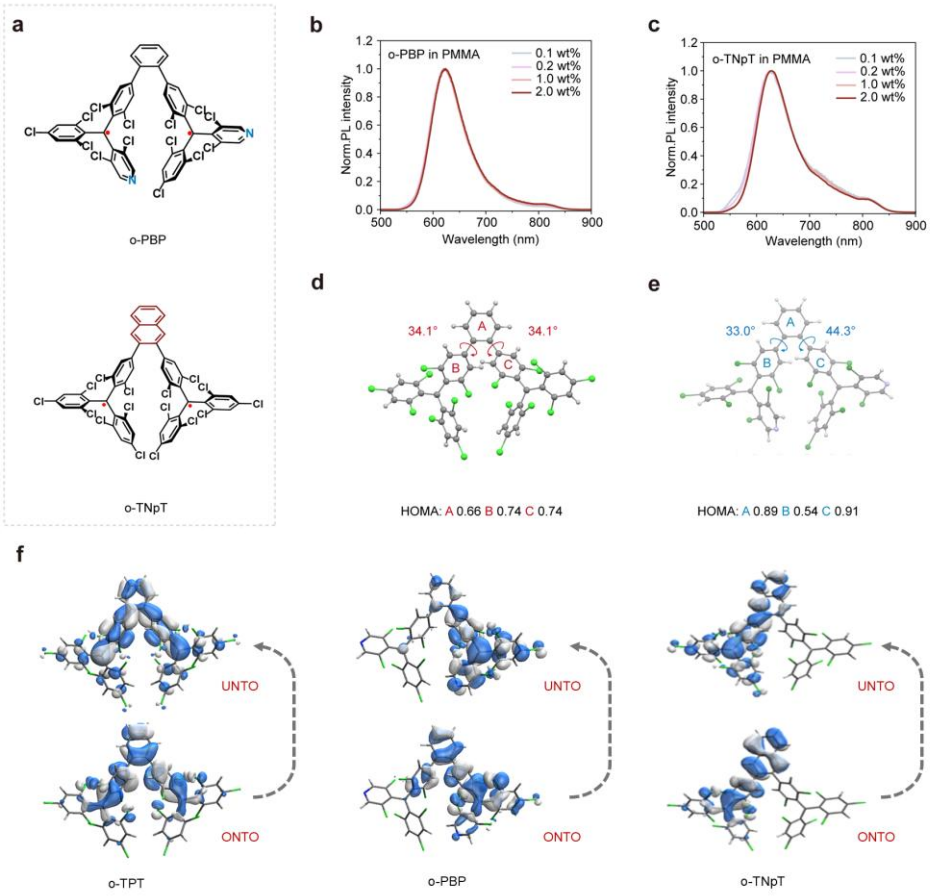


Fig. 4 | Structural Requirements for Excited-State Quinoidization and efficient singlet emission. a, Molecular structures of the control diradicals o-PBP (top) and o-TNpT (bottom). **b**, **c**, Photoluminescence (PL) spectra of o-PBP (b) and o-TNpT (c) in PMMA films at doping concentrations of 0.1-2 wt%, measured at room temperature. **d**, **e**, Optimized triplet excited-state geometries from TD-UDFT calculations: o-TPT (d) o-PBP (e). **f**, occupied NTO (ONTO) and unoccupied NTO (UNTO) analysis of the T_1 excited state of the three diradicals at their respective T_1 optimized geometries, from TD-UB3LYP/def2SVP calculations.

resolving the effect of connectivity.

Additional NEVPT2 calculations at both the SE and DE optimized geometries confirm that the optically allowed SE state remains below the DE state (Supplementary Fig. 23). Orbital analysis (Supplementary Fig. 24) reveals comparable bridge participation in Müller and o-TPT, accompanying a quinoidal distortion which, for o-TPT provides the structural rigidification that preserve molecular symmetry in the excited state optimized structure. This symmetry maintains the distinct SE and DE characters of the two CR states and the substantial oscillator strength of SE (Fig. 5a), whereas symmetry breaking would enable SE-DE mixing to form a localized CT state with weaker optical activity. Interestingly, these results agree with the observed characteristics of this S_1 excited state which also exhibits significant differences from known zwitterionic states. Reported luminescent zwitterionic emissive diradicals[31,34,37,39,42,43,46] typically exhibit long fluorescence lifetimes (~70 ns) and pronounced solvatochromic effects. In marked contrast, the lowest energy band of o-TPT shows a fluorescence lifetime of merely 11-14 ns (Supplementary Table. 4), much shorter than those reported for zwitterionic emissive states

Structural Requirements for Excited-State Quinoidization and efficient singlet emission.

To identify the structural factors responsible for the emergence of the singlet state featuring SE/CR character, we designed two complementary control diradicals (Fig. 4a). In o-PBP, the TTM radicals were substituted with the more electron-withdrawing PyBTM units, thereby modifying the electronic structure without altering the overall ortho-linked diradical topology. In o-TNpT, the central phenylene bridge was replaced by a naphthalene unit to enhance and aromatic stabilization of the bridging framework while preserving the TTM radical termini. Together, these two control molecules enable independent evaluation of the roles of the bridging framework and radical electronic structure in governing the excited-state behaviors.

Both o-PBP and o-TNpT exhibit characteristic diradical signa tures in EPR measurements, including a well-defined central reson ance signal and a detectable half-field transition in PMMA films (S upplementary Fig. 9), confirming the formation of triplet diradical species. Moreover, their absorption spectra closely resemble that of o-TPT (Supplementary Fig. 11), indicating that these structural m odifications do not fundamentally alter the overall electronic excita tion manifold. Despite these similarities, the three diradicals displa y markedly different photophysical behaviors. Whereas o-TPT con sistently exhibits dual emission in PMMA films (Fig. 2b), both o-P BP (Fig. 4b) and o-TNpT (Fig. 4c) display only a single emission ba

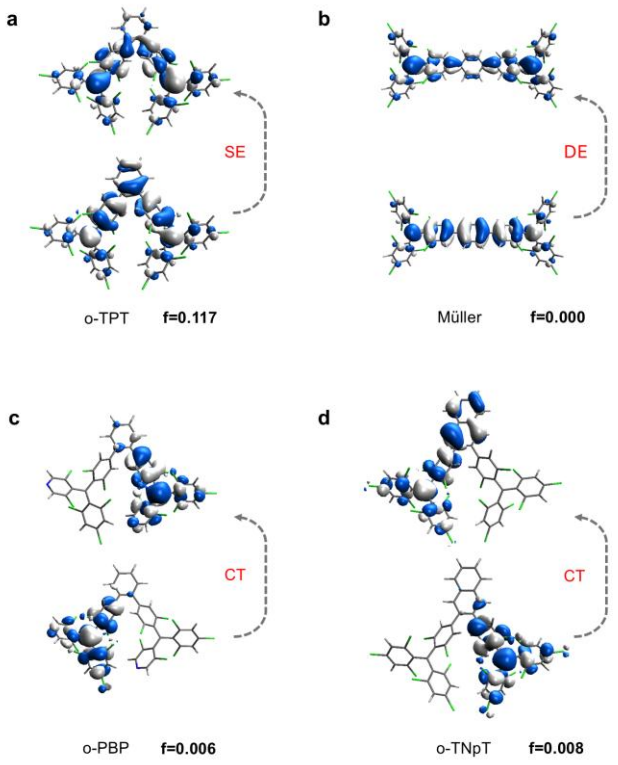


Fig. 5| Potential applications of chiral exciplex under different conditions. The lowest singlet excited state: dominant excitation, orbital character and predicted oscillator strength for **a**, o-TPT where SE/DE inversion occurs; **b**, Müller diradical where DE is the lowest singlet **c**, o-PBP (b) and **d**, o-TNpT where symmetry breaking occurs leading to a CT states, From CASSCF/NEVPT2 calculations.

nd (i.e., TTM-like or LE emission around 620 nm) throughout the i nvestigated concentration range. Only a weak feature around 800 n m is observed

Consistent with this picture, triplet emission persists, whereas singlet emission is absent or very weak in o-PBP and o-TNpT. Given the distinct orbital characters of the two emit-ting states in o-TPT, this behavior suggests that changes to the bridge or radical centers more strongly affect the photophysics of the lowest CR singlet states than the LE triplet state.

Geometry optimizations of both the ground and excited states reveal a common structural evolution shared by all three molecules. Each adopts a highly twisted aromatic configuration in the ground state (Supplementary Tables. 6,7 and 10-13). Concerning the lowest excited triplet state, all three exhibit a pronounced tendency toward quinoidal structural reorganization, as reflected by reduced dihedral angles, enhanced ortho-conjugation, and consistently decreased HOMA values in the involved phenyl rings (Supplementary Fig. 26).

Despite this shared tendency, the three diradicals ultimately evolve toward fundamentally different relaxed excited-state structures. In o-TPT, the excited-state relaxation proceeds in a globally symmetric manner. The dihedral angles between the central phenylene ring (ring A) and the adjacent aryl units decrease cooperatively from ap-proximately 50° in the ground state to 34° in the relaxed excited state (Fig. 4d and Supplementary Figs. 26a, d), accompanied by concerted planarization of the entire molecular framework, yielding a fully quinoidal excited-state geometry. Simultaneously, the HOMA values of rings A-C decrease from 0.94, 0.90, and 0.90 in the ground state to 0.66, 0.74, and 0.74, respectively (Supplementary Figs. 26a, d), demonstrating a substantial concomitant reduction in aromaticity and the establishment of pronounced quinoidal character. In contrast, o-PBP and o-TNpT only exhibit unilateral, localized quinoidal distortion on one fragment of the molecule (Fig. 4e, and Supplementary Figs. 26b, c and e, f).

The NTO analysis at the T_1 optimized geometry of the three diradicals is shown in Fig 4f. The extension of the occupied and unoccupied NTO on the bridge of o-PBP and o-TNpT favors a quinoidal structure but in both cases the symmetry is broken. For o-PBP, the origin of the broken symmetry is straightforward. First, the inclusion of the pyridine can significantly stabilize the TTM radical by the inclusion of additional captodative effect, with mesomeric and inductive stabilizations, which suppresses the delocalization of the unpaired electrons toward the central benzene ring. In addition, after optimizing all possible torsional arrangements of the pyridine rings and selecting the lowest-energy con-former as the ground-state structure (Supplementary Fig. 25), the T_1 excited state localizes the excitation as shown by the NTO analysis in Fig. 4f.

Similar symmetry breaking and localization of the excitation on a single molecular moiety occur in o-TNpT. At the same time, the nodal patterns of the bridge orbitals may weaken mixing with the radical-centered orbitals involved in the CR states, limiting bridge participation and the associated quinoidal distortion only on one side of the molecule (Supplementary Figs. 26c, f).

The calculated oscillator strengths for $T_1 \rightarrow T_0$ emission are comparable across the three diradicals (Supplementary Table. 8), consistent with the observation of triplet emission in all three systems. Localization therefore does not substantially diminish the transition strength of these predominantly LE triplet states. A different response may be expected in the singlet manifold, given the CR character of the relevant excitations.

The negligible singlet emission in o-PBP and o-TNpT may reflect a lower intrinsic singlet emission efficiency, a reduced population transfer from S_1 to T_1 via intersystem crossing (ISC), or both. We investigated the intrinsic emission efficiency at CASSCF/NEVPT2 level, in comparison to o-TPT. The excitation energies and oscillator strengths of the S_1 state are compiled in Supplementary Table 14, In the singlet manifold a different situation emerges for o-PBP and o-TNpT, where singlet excited-state geometry optimization (Supplementary Fig. 27) leads to a pronounced loss of molecular symmetry compared to o-TPT, similarly to the triplet excited state. In both compounds, the less effective electronic interaction between the bridge and the radical centers prevents the cooperative, symmetry-preserving structural relaxation observed for o-TPT, although the underlying reasons differ. In o-PBP, the different orientations of the radical units, together with the electron-withdrawing character of the pyridyl substituents, favor an asymmetric redistribution of the electronic density. In o-TNpT, instead, the nodal topology of the naphthalene bridge orbitals limits their effective mixing with the radical-centered orbitals, hindering the development of a globally delocalized quinoidal structure. In both cases, the resulting symmetry breaking

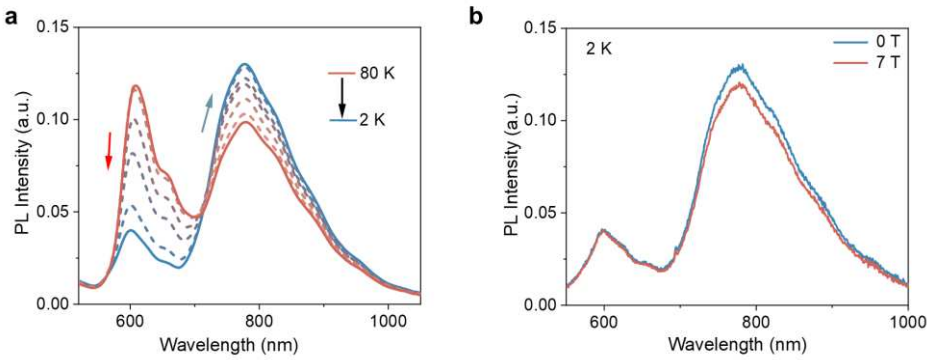


Fig. 6| Temperature- and magnetic-field-dependent PL spectra of o-TPT. a, Temperature-dependent PL spectra of 0.2 wt% o-TPT/PMMA from 2 to 80 K. **b**, Comparison of PL spectra under 0 T and 7 T at 2 K.

promotes mixing between the SE and DE charge-resonance configurations, yielding a lowest singlet excited state with a more localized, zwitterionic CT character (Fig 5 and Supplementary Fig. S28) and a reduced contribution from the bridge all together removing a large fraction of emissive character. Unlike the SE state of o-TPT, which shows a large oscillator strength, these symmetry-broken states exhibit substantially weaker NEVPT2 computed radiative activity. The contrasting behavior of the three diradicals therefore highlights the importance of bridge-mediated electronic coupling and symmetry-preserving structural relaxation in maintaining a strongly emissive low-energy singlet state.

Temperature-Modulated Emission and Magnetoluminescence Response

With the identity of the emissive state clarified by the preceding structural and orbital investigations, we turn to examine the role of spin-state dynamics by means of temperature-dependent photoluminescence. Temperature-dependent photoluminescence measurements reveal that the two emission bands exhibit divergent responses to thermal perturbation in Fig. 6a. Upon cooling from 300 K to 80 K, the intensities of both emission bands increase simultaneously (Supplementary Fig. 29), which is ascribed to the suppression of nonradiative decay channels. In contrast, further cooling from 80 K to 2 K leads to differentiated spectral evolution: the low-energy emission continuously intensifies, while the high-energy emission gradually diminishes (Fig. 6a).

This distinctive temperature dependence indicates thermally activated population exchange between the singlet and triplet excited-state manifolds. Vertical excitation calculations at the ground-state equilibrium geometry reveal that the TTM-like triplet locally excited state (T_1) is nearly degenerate with the singlet state (S_3), which provides a channel for thermally activated intersystem crossing (ISC in Fig. 3b) and dynamically modulates the relative populations of these two excited states (Supplementary Fig. 30). Between 300 K and 80 K, thermal quenching dominates excited-state decay. Cooling suppresses nonradiative decay channels, leading to concurrent enhancement of both emission bands. Upon further cooling from 80 K to 2 K, the thermally activated ISC process is markedly suppressed, leading to the redistribution of excited-state populations: the population fraction of T_1 decreases while that of the singlet state increases accordingly. This mechanism is consistent with the variable-temperature spectroscopic results: the triplet emission at 618 nm assigned to the $T_1 \rightarrow T_0$ transition diminishes, accompanied by a concurrent enhancement of the singlet emission at 780 nm originating from the $S_1 \rightarrow S_0$ transition.

To unravel the magnetic-field-responsive excited-state relaxation pathway of o-TPT/PMMA films, magnetoluminescence measurements were performed. Upon application of an external magnetic field at 2 K, the field selectively quenches the 780 nm singlet emission band assigned to the bright SE state, whereas the high-energy triplet emission at 618 nm originating from the TTM-like localized excited T_1(LE) state remains nearly unaffected (Fig.6b). Identical trends are observed at 7 K and 15 K (Supplementary Fig. 31), which rules out the conventional magnetic-field-modulated intersystem crossing (ISC) pathway. A possible mechanism for this observation is that the external magnetic field perturbs the electronic symmetry of the π-electron system via spin-vibronic coupling.[47] This symmetry perturbation induces partial configuration mixing between the bright SE singlet state and dark DE singlet state. Such mixing accelerates nonradiative internal conversion (IC) from the S_1 state back to the ground state S_0 and reduces the oscillator strength of the emissive SE state. In contrast, the T_1 triplet state is dominated by localized excitation (LE) centered on the TTM subunit, and its radiative channel does not rely on the global SE/DE symmetry. Magnetic-field-induced SE/DE mixing essentially corresponds to spatial symmetry breaking within the singlet manifold, serving as a nonradiative dissipation pathway confined to singlet states and thus does not substantially modify the T_1 population, rendering the 618 nm triplet emission insensitive to the magnetic field macroscopically.

Discussion

In summary, we demonstrate that ortho-disubstitution provides an effective molecular design strategy to reverse the SE/DE ordering, placing the bright SE state lowest and enabling singlet luminescence in an open-shell Kekulé diradical. Unlike conventional para-disubstituted diradicals, where the SE excited state is pushed to higher energy and rendered optically inactive by excited-state electronic reordering, o-TPT restores this state as a radiatively accessible emissive channel through cooperative global electronic redistribution and symmetry preserved during structural relaxation. Structural, magnetic, spectroscopic, and theoretical analyses

consistently show that o-TPT adopts a highly twisted aromatic open-shell ground-state configuration with pronounced diradical character and an almost degenerate triplet ground state. Owing to the small singlet-triplet energy gap, singlet and triplet ground-state species coexist in thermal equilibrium, allowing photoexcitation of both spin manifolds and giving rise to two independent emissive pathways. Comparative studies of structurally related diradicals further reveal that the reverse of the SE/DE state ordering requires both efficient global electronic redistribution and preservation of molecular symmetry during excited-state relaxation, thereby defining the electronic and structural requirements for lowering the SE luminescent state. Variable-temperature and magnetoluminescence measurements further demonstrate that the excited states actively participate in spin-dependent relaxation processes, revealing a close interplay between excited-state electronic structure, molecular geometry, and spin dynamics. More broadly, this work establishes a new conceptual framework for designing emissive open-shell diradicals by reversing the DE/SE order of the lowest singlet excited states. Beyond the specific molecular platform investigated here, our results demonstrate that dual emission can serve as a direct spectroscopic probe for visualizing otherwise inaccessible excited-state electronic structure evolution, opening new opportunities for understanding and engineering excited-state processes in organic open-shell molecular systems.

Online content

Any methods, additional references, Nature Portfolio reporting summaries, source data, extended data, supplementary information, acknowledgements, peer review information; details of author contributions and competing interests; and statements of data and code availability are available at

References

1 Kodama, T. et al. Molecular and spin structures of a through-space conjugated triradical system. *Angew. Chem. Int. Ed.* **61**, e202200688. (2022).

2 Mizuno, A.; Matsuoka, R.; Mibu, T.; Kusamoto, T., Luminescent radicals. *Chem. Rev.* **124**, 1034-1121 (2024).

3 Konrai, S. et al. Photochemical and thermal concerted 1,3-sigmatropic rearrangements of a ⊓-extended methylenecyclopro-pane. *J. Am. Chem. Soc.* **147**, 38700-38710 (2025).

4 Murto, P. et al. Mesitylated trityl radicals, a platform for doublet emission: symmetry breaking, charge-transfer states and conjugated polymers. *Nat. Commun.* **14**, 4147 (2023).

5 Mamusi, F., Ribas-Ariño, J., Deumal, M., Fumanal, M. The role of charge transfer and linker states in the magnetoluminescence of a diradical with two spatially proximate triarylmethyl units. *Adv. Opt. Mater.* e71435 (2026).

6 (1) Biswas, S., Sandwisch, J. W., Weakly, R. B., Khalil, M., Tracking coherent vibronic and vibrational motions in ultrafast proton transfer. *Nat. Commun.* doi: 10.1038/s41467-026-72661-9 (2026).

7 Liu, G. et al. Symmetry-broken intermolecular charge separation of cationic radicals. *Angew. Chem. Int. Ed.* **62**, e202301348 (2023).

8 Huang, T. et al. Manipulation of intramolecular charge transfer in NIR-II emissive organic diradicaloids via a symmetry-breaking design. *Chem.* **11**, 102621 (2025).

9 Ball, R. et al. Excited-state symmetry breaking dynamics driven by mode-resolved Jahn–Teller distortion in luminescent tris(2,4,6-trichlorophenyl)methyl radicals. *J. Am. Chem. Soc.* **148**, 22025–22035 (2026).

10 Nishiuchi, T., Aibara, S., Sato, H. & Kubo, T. Synthesis of π-extended Thiele's and Chichibabin's hydrocarbons and effect of the π-congestion on conformations and electronic states. *J. Am. Chem. Soc.* **144**, 7479–7488 (2022).

11 Houplin, A., Liu, C.-H. & Perepichka, D. F. Designing stable π-radicals. *Chem. Soc. Rev.* 55, 7999–8034 (2026).

12 Di Motta, S., Negri, F., Fazzi, D., Castiglioni, C. & Canesi, E. V. Biradicaloid and polyenic character of quinoidal oligothiophenes revealed by the presence of a low-lying double-exciton state. *J. Phys. Chem. Lett.* **1**, 3334–3339 (2010).

13 Canola, S., Casado, J. & Negri, F. The double exciton state of conjugated chromophores with strong diradical character: insights from TDDFT calculations. *Phys. Chem. Chem. Phys.* **20**, 24227–24238 (2018).

14 Abe, M. Diradicals. *Chem. Rev.* **113**, 7011–7088 (2013).

15 Konishi, A. & Kubo, T. Benzenoid quinodimethanes. *Top. Curr. Chem.* **375**, 83 (2017).

16 Stuyver, T. et al. Do diradicals behave like radicals? *Chem. Rev.* **119**, 11291–11351 (2019).

17 Li, G. et al. Toward stable superbenzoquinone diradicaloids. *Angew. Chem. Int. Ed.* **56**, 5012–5016 (2017).

18 Hu, X., Wang, W., Wang, D. & Zheng, Y. The electronic applications of stable diradicaloids: present and future. *J. Mater. Chem. C.* **6**, 11232–11242 (2018).

19 Abdurahman, A. et al. A highly stable organic luminescent diradical. *Angew. Chem. Int. Ed.* **62**, e202300772 (2023).

20 Zhu, Y., Zhu, Z., Wang, S., Peng, Q. & Abdurahman, A. Stable luminescent diradicals: the emergence and potential applications. *Angew. Chem. Int. Ed.* **64**, e202423470 (2025).

21 Chang, X. et al. A stable Chichibabin diradicaloid with near-infrared emission. *Angew. Chem. Int. Ed.* **63**, e202404853 (2024).

22 Zhu, Z. et al. Dual channel emissions of Kasha and anti-Kasha from a single radical molecule. *Angew. Chem. Int. Ed.* **63**, e202410552 (2024).

23 Hattori, Y., Yamamoto, K., Kitajima, R. & Uchida, K. Bright fluorescent p-phenylene-bridged triarylmethyl highly stable diradical. *Chem. Eur. J.* **30**, e202304124 (2024).

24 Konishi, A. & Kubo, T. Benzenoid quinodimethanes. *Top. Curr. Chem.* **375**, 83 (2017).

25 Dressler, J. J. et al. Thiophene and its sulfur inhibit indenoindenodibenzothiophene diradicals from low-energy lying thermal triplets. *Nat. Chem.* **10**, 1134–1140 (2018).

26 Barker, J. E. et al. Molecule isomerism modulates the diradical properties of stable singlet diradicaloids. *J. Am. Chem. Soc.* **142**, 1548–1555 (2020).

27 Sun, Z. et al. Dibenzoheptazethrene isomers with different biradical characters: an exercise of Clar's aromatic sextet rule in singlet biradicaloids. *J. Am. Chem. Soc.* **135**, 18229–18236 (2013).

28 Jiao, T. et al. Solution-phase synthesis of Clar's goblet and elucidation of its spin properties. *Nat. Chem.* **17**, 924–932 (2025).

29 Gorgon, S. et al. Reversible spin-optical interface in luminescent organic radicals. *Nature.* **620**, 538–544 (2023).

30 Kopp, S. M. et al. Luminescent organic triplet diradicals as optically addressable molecular qubits. *J. Am. Chem. Soc.* **146**, 27935–27945 (2024).

31 Chowdhury, R. et al. Bright triplet and bright charge-separated singlet excitons in organic diradicals enable optical read-out and writing of spin states. *Nat. Chem.* **17**, 1410–1417 (2025).

32 Liu, T. et al. Efficient luminescent stable Chichibabin diradicaloid for near-infrared imaging and photothermal therapy. *Light Sci. Appl.* **14**, 289 (2025).

33 Tong, Z. et al. Deciphering spin-governed dual emissions in TTM diradicaloids: unraveling the interplay of singlet and triplet fluorescence pathways. *J. Am. Chem. Soc.* **147**, 39232–39246 (2025).

34 Mesto, D. et al. Luminescent trityl-based diradicaloids: a theoretical and experimental assessment of charge-resonance in low-lying excited states. *Chem.*

Eur. J. e202500749 (2025).

35 Mamusi, F., Ribas-Ariño, J., Deumal, M. & Fumanal, M. The role of charge transfer and linker states in the magnetoluminescence of a diradical with two spatially proximate triarylmethyl units. *Adv. Opt. Mater.* **14**, e71435 (2026).

36 Matsuoka, R., Kimura, S., Miura, T., Ikoma, T. & Kusamoto, T. Single-molecule magnetoluminescence from a spatially confined persistent diradical emitter. *J. Am. Chem. Soc.* **145**, 13615–13622 (2023).

37 Matsuoka, R. et al. Spectroscopic characterization of the charge-separated zwitterionic state responsible for the excimer-like emission of a luminescent diradical. *J. Am. Chem. Soc.* **148**, 1086–1095 (2026).

38 Zhou, Z. et al. Sulfone-functionalized Chichibabin's hydrocarbons: stable diradicaloids with symmetry breaking charge transfer contributing to NIR emission beyond 900 nm. *J. Am. Chem. Soc.* **146**, 6763–6772 (2024).

39 Bevilacqua, M. et al. Hidden diradical: conformational switch for solvatochromic NIR emission with unity quantum yield in Thiele's hydrocarbon. *Angew. Chem. Int. Ed.* **65**, e24042 (2026).

40 Dong, S. et al. Extended bis(benzothia)quinodimethanes and their dications: from singlet diradicaloids to isoelectronic structures of long acenes. *Angew. Chem. Int. Ed.* **55**, 9316–9320 (2016).

41 Ni, Y. et al. 3D global aromaticity in a fully conjugated diradicaloid cage at different oxidation states. *Nat. Chem.* **12**, 242–248 (2020).

42 Liu, C.-H. et al. Thiele's fluorocarbons: stable diradicaloids with efficient visible-to-near-infrared fluorescence from a zwitterionic excited state. *J. Am. Chem. Soc.* **145**, 15702–15707 (2023).

43 Punzi, A. et al. Dark state of the Thiele hydrocarbon: efficient solvatochromic emission from a nonpolar centrosymmetric singlet diradicaloid. *J. Am. Chem. Soc.* **145**, 20229–20241 (2023).

44 Kimura, S. et al. Magnetoluminescence in a photostable, brightly luminescent organic radical in a rigid environment. *Angew. Chem. Int. Ed.* **57**, 12711–12715 (2018).

45 Kato, K., Kimura, S., Kusamoto, T., Nishihara, H. & Teki, Y. Luminescent radical-excimer: excited-state dynamics of luminescent radicals in doped host crystals. *Angew. Chem. Int. Ed.* **58**, 2606–2611 (2019).

46 Punzi, A. et al. Twist and shine: the impact of halogen substitution on Thiele hydrocarbon's optical properties. *Angew. Chem. Int. Ed.* **65**, e24043 (2026).

47 Mariano, L. A., Mondal, S. & Lunghi, A. Spin-vibronic dynamics in open-shell systems beyond the spin Hamiltonian formalism. *J. Chem. Theory Comput.* **20**, 323–332 (2024).

Methods

Materials

Thin film preparation.

Poly(methyl methacrylate) (PMMA) was dissolved in chromatographic-grade dichloromethane to prepare a polymer stock solution. Radical compounds were added at concentrations of 0.1–2 wt% relative to the PMMA mass, followed by ultrasonication for 10 min to ensure homogeneous dispersion. The resulting solutions were drop-cast onto pre-cleaned quartz substrates (10 × 10 × 1 mm) and dried under ambient conditions to afford optically transparent doped PMMA films for photophysical measurements.

EPR measurements

Continuous-wave (CW) electron paramagnetic resonance (EPR) spectra and variable-temperature EPR measurements were recorded on a Bruker ELEXSYS II E500 spectrometer. Thin-film samples were scraped from the substrates and loaded into Spectrosil® quartz EPR tubes (3 mm inner diameter). Variable-temperature measurements were performed under liquid-nitrogen cooling.

SQUID magnetometry

Magnetic measurements were carried out on a Quantum Design MPMS®3 SQUID magnetometer. Samples were mounted in gelatin capsules and placed in standard straw sample holders. Magnetization data were collected under zero-field-cooled conditions.

Optical spectroscopy

UV–Vis absorption spectra were recorded on a Shimadzu UV-2550 double-beam spectrophotometer. Steady-state photoluminescence spectra were measured on a Hitachi F-4700 fluorescence spectrometer using 375 nm excitation. Fluorescence lifetimes and photoluminescence quantum yields (PLQYs) were measured on an Edinburgh FLS980 steady-state/transient fluorescence spectrometer equipped with an integrating sphere. Time-resolved measurements were performed using the time-correlated single-photon counting (TCSPC) technique, and fluorescence decay curves were analyzed by multi-exponential fitting.

Transient absorption spectroscopy

Ultrafast transient absorption (TA) spectroscopy was performed to investigate the excited-state dynamics of o-TPT. Pump pulses at 375 nm (<200 fs) were generated using a Light Conversion PH2-10W femtosecond laser system equipped with an ORPHEUS-HP optical parametric amplifier. Broadband white-light probe pulses (480–950 nm) were generated using a YAG crystal and detected with a TA100 transient absorption spectrometer (Chuangrui Spectroscopy). Samples were prepared as 2 wt% o-TPT-doped PMMA films. Transient spectra were collected over a delay time range of 2 to 7000 ps.

Theoretical calculations

Vertical electronic excitations were characterized using three distinct computational protocols. First, TD-UDFT calculations at the TD-UB3LYP/6-31G(d,p) and TD-UB3LYP/def2SVP levels were performed on the optimized S_0 and T_0 geometries to obtain excitation energies, followed by electron–hole analyses and NTO investigations for identifying SE and DE states. Second, CASSCF(4,4) state-averaged calculations were carried out to describe the essential orbital interactions between radical centers and bridging units. Third, NEVPT2 corrections were applied on top of the CASSCF wavefunctions to incorporate dynamic electron correlation effects. Further computational details are provided in Section S6 of the Supporting Information.

Variable-temperature and magnetoluminescence measurements

Variable-temperature photoluminescence and magnetoluminescence measurements were performed using a SpectromagPT superconducting magneto-optical system (Oxford Instruments) equipped with a variable-temperature cryostat. Measurements were carried out over magnetic fields of 0–7 T and temperatures between 2 and 300 K. Samples were excited using a 365 nm LED, and the emitted photoluminescence was collected with an Ocean Optics QE65 Pro fiber-optic spectrometer.

Data availability

The data supporting the findings of this study are available in the main text, the Supplementary Information, and the accompanying Source Data file. Crystallographic data have been deposited at the Cambridge Crystallographic Data Centre (CCDC) under deposition numbers 2526754 (o-HTPT) and 2526749 (o-TPT) (see Supplementary Table 1) and can be obtained free of charge via https://www.ccdc.cam.ac.uk/data_request/cif. Source data are provided with this paper.

Acknowledgements

We gratefully thank the National Natural Science Foundation of China (Grant No. 62422404, 52103210, 62475116, U24A20292), the Natural Science Foundation of Jilin Province (Grant No. 20230101363JC). JC acknowledges financial support from MICINN/AEI of Spain (project number PID2024-157601NB-I00).

Author contributions

A.A. conceived the project, designed the research, supervised the study, interpreted the results, and wrote the manuscript. Z.D. and Z.Z. performed the experiments, analyzed the data, and prepared the original draft of the manuscript. Y.S. carried out the SQUID magnetometry measurements. X.W. performed the transient absorption spectroscopy measurements and, together with S.W., carried out the variable-temperature and magnetoluminescence measurements. F.N. performed the key theoretical calculations, contributed substantially to the interpretation of the excited states, and revised the manuscript. J.C. contributed to the conceptual development of the work, established the theoretical framework for interpreting the excited-state electronic structure and photophysical mechanism, and substantially revised the manuscript. Q.P. and X.A. contributed to data interpretation and manuscript revision. All authors discussed the results and commented on the manuscript.

Competing interests

The authors declare no competing interests.

Additional information

Supplementary information is available for this paper in the online version of the paper.

Reprints and permission information is available online at www.nature.com/reprints

Correspondence and requests for material should be addressed to Alim Abdurahman

Supplementary Files

This is a list of supplementary files associated with this preprint. Click to download.

- Supplementarymaterials.docx